HHS Public Access

Author manuscript

Contrast Media Mol Imaging. Author manuscript; available in PMC 2019 April 26.

Published in final edited form as:

Contrast Media Mol Imaging. 2012 ; 7(2): 247–253. doi:10.1002/cmmi.489.

MR and optical imaging of early micrometastases in lymph nodes: triple labeling with nano-sized agents yielding distinct signals

Nobuyuki Kosaka[a], **Marcelino Bernardo**[a,b], **Makoto Mitsunaga**[a], **Peter L. Choyke**[a], and **Hisataka Kobayashi**[a,*]

[a] Molecular Imaging Program, Center for Cancer Research, National Cancer Institute, National Institutes of Health, Bethesda, MD, 20892-1088, USA

[b] Research Technology Program, SAIC-Frederick Inc., NCI-Frederick, National Institutes of Health, Frederick, MD, 21702, USA

Abstract

Few imaging methods are available for depicting *in vivo* cancer cell migration within the lymphatic system. Detection of such early micrometastases requires extremely high target to background. In this study, we dual-labeled human breast cancer cells (MDA-MB468) with a small particle of iron oxide (SPIO) and a quantum dot (QD), and tracked these cells in the lymphatic system in mice using *in vivo* MRI and optical imaging. A generation-6 gadolinium-dendrimer-based MRI contrast agent (Gd-G6) was employed for visualizing regional lymphatic channels and nodes. Since Gd-G6 shortened T_1 leading to high signal, whereas SPIO-labeled cancer cells greatly lowered signal, a small number of cells were simultaneously visualized within the draining lymphatic basins. One million dual-labeled cancer cells were subcutaneously injected into the paws of mice 24h prior to imaging. Then whole body images were acquired pre- and post-intracutaneous injection of Gd-G6 with 3D-T_1w-FFE and balanced-FFE sequences for cancer cell tracking and MR lymphangiography. *In vivo* MRI clearly visualized labeled cancer cells migrating from the paw to the axillary lymph nodes using draining lymphatics. *In vivo* optical imaging using a fluorescence surgical microscope demonstrated tiny cancer cell clusters in the axillary lymph node with high spatial resolution. Thus, using a combination of MRI and optical imaging, it is possible to depict macro- and early micrometastases within the lymphatic system. This platform offers a versatile research tool for investigating and treating lymphatic metastases in animal models.

Keywords

iron oxide nanoparticle; quantum dots; lymphatic metastasis; dendrimer; MRI

[*]Correspondence to: Hisataka Kobayashi, Molecular Imaging Program, National Cancer Institute, NIH, Building 10, Room B3B69, MSC1088, Bethesda, MD 20892–1088, USA. Kobayash@mail.nih.gov.

1. INTRODUCTION

The lymphatic system is difficult to visualize because it is much less accessible than the vascular system (1). Various nano-materials have been used *in vivo* to investigate the lymphatics using interstitial injections, whereby the contrast agent is absorbed and transported from the interstitial tissue into the collector lymphatics (2–4). A particularly vexing issue is the study of cancer cell migration into and through the lymphatics. These cancer cells take advantage of the enlarged and porous lymphatics found after tumor lymphangiogenesis (5). The detection of small numbers of cells within the tiny lymphatics *in vivo* requires very high target-to-background ratios (TBR). The visualization of cancer cells can be achieved by labeling the cells with iron oxide nanoparticles that are detectable with MRI (6). However, without delineating the lymphatic system, it is impossible to verify the location of the tagged cells. Therefore, a method of enhancing the lymphatic structures is also necessary to achieve sufficient TBR. Nanoparticles such as iron oxides and dendrimers are well suited to study of the lymphatics, not only because of the size-selectivity of the lymphatic system, but also because of the enhanced signals that derive from larger particles. For example, superparamagnetic iron oxide (SPIO) nano-particles can increase R_2* more than >30-fold at 1.5 T and higher under greater magnetic field strength (7), and gadolinium-dendrimer-molecules can increase R_1 more than 10 000-fold compared with small gadolinium-chelates (8,9). Therefore, low concentrations of these particles or molecules can be detected with MRI. For optical imaging quantum dots (QD) can increase light emission by more than 100-fold compared with small organic fluorophores at similar wavelengths, which enables real-time observation (10). Thus, these nanoparticles have particular advantages when imaging clusters of migrating cancer cells, which will originate micrometastases in the lymphatics.

Multiplexed imaging, which uses two or more modalities, has become a powerful approach in both the laboratory and clinic for obtaining accurate and precise information *in vivo* (11). By using more than one modality, multiplexed imaging can overcome the limitations of each modality when used alone. For instance, combined use of nuclear and optical imaging provides high-sensitivity (optical) and quantitation (nuclear) images during a single imaging session (12). Simultaneous use of multiple optical agents can depict different targets (13) or different lymphatic basins (14).

To visualize cancer cell migration in the lymphatic system, we simultaneously employed three different nano-sized agents: an SPIO and QD to label breast cancer cells for tracking by MRI and optical imaging, respectively, and a generation-6 gadolinium-dendrimer-based MRI contrast agent (Gd-G6) for MR lymphangiography. Simultaneous use of a negative signal in the cells (SPIO to shorten T_2*) and a positive MR contrast agent (Gd-G6 to shorten T_1) can visualize the small clusters of labeled cancer cells within the draining lymphatic basins. Furthermore, additional labeling of QD provides higher spatial resolution using intravital surgical microscopy.

2. RESULTS

2.1. *In vitro* validation of dual-labeling

Confirmation of the dual-labeling of MDA-MB468 cells was performed with fluorescence microscopy and Prussian blue staining (iron staining). Dual-labeled cancer cells clearly incorporated both iron and QD within their cytoplasm, while nonlabeled control cells did not (Fig. 1A). To further evaluate the efficiency of labeling, two-color flow cytometry was also performed with dextran-staining, which fluorescently stained the SPIO using a monoclonal antibody. Flow cytometry demonstrated successful dual labeling in 90.1 ± 7.1% of cells (Fig. 1B). Quantification of intracellular iron labeled cells was performed with UV–vis spectrometric methods. Dual-labeled cells contained 11.61 ± 1.59 pg iron per cell, while almost no iron was detected in nonlabeled control cells (0.04 ± 0.35 pg iron per cell). Viability was assessed with the trypan blue exclusion method. Dual-labeled cells and SPIO-labeled cells showed slightly lower viability (87.8 ± 3.3 and 89.7 ± 2.6%, respectively) than nonlabeled control cells and QD-labeled cells (92.7 ± 2.1 and 92.4 ± 2.1%, respectively). These differences were statistically significant ($P < 0.05$, Kruskal–Wallis test with Dunn's multiple comparisons test).

2.2. Intralymphatic cancer cell tracking with MR and optical imaging *in vivo*

In vivo cell tracking was performed under MRI, followed by *in vivo* optical imaging. Twenty-four hours after dual-labeled cancer cell inoculation in the left paw, T_1-weighted fast field echo (T_1w-FFE) images showed a dark signal in the periphery of the left axillary lymph node (Fig. 2B), corresponding to SPIO-labeled cancer cells. After administration of Gd-G6 MR contrast agents into the left paw, the lymphatic basin was depicted with the SPIO labeled cells starkly depicted against a bright background (negative enhancement, cancer cells; positive enhancement, lymphatic basin). In contrast, no enhancements (neither negative nor positive) were observed in the contralateral axillary lymph node. The identical findings were also observed with balanced-steady-state free precession (b-FFE) MR images (Fig. 2B).

Following MR imaging, *in vivo* optical imaging was performed with a macro-zoom fluorescence microscope. Fluorescence images showed optically labeled cancer cell clusters (small red dots in Fig. 2 C) in the left axillary lymph node with high spatial resolution. These labeled cancer cells could be observed in real time owing to bright fluorescence from QDs (see video in Supporting Information). After optical imaging, mice were euthanized and histological validation of labeled-cancer cells was performed with hematoxylin–eosin (H-E) staining, Prussian-blue staining and fluorescence microscopy. These images confirmed the presence of dual-labeled cancer cells in the peripheral of left axillary lymph node, corresponding to the *in vivo* images (Figure 3).

3. DISCUSSION

Cancer spread into the lymphatic system is a significant prognostic factor in most cancer patients (15,16), and therefore, it is important to understand how cancer cells migrate within the lymphatic system (17). *In vivo* cell tracking, including macrophages, stem cells and

cancer cells, has been applied in many preclinical studies and has proved to be a robust tool for biomedical research. Currently two major techniques are commonly used for cell tracking: MR imaging with a SPIO and optical imaging with fluorophores or fluorescence proteins (18–21). SPIO is a nano-sized iron oxide particle, which is coated by dextran. Once target cells ingest SPIO within their cytoplasm, even very small numbers of cells (~600 cells per voxel) can be detected owing to the strong susceptibility effects of incorporated iron (22). When labeled with micron-sized iron oxide particles, a single cell can be detected with a high magnetic field scanner (23). Another technique is optical imaging that uses a super-bright inorganic fluororescent nano-particle (e.g. QD) or fluorescence proteins, which emit bright fluorescence from labeled target cells. Cell tracking is therefore feasible; however, tracking cancer cells within the lymphatic system is still limited, since it can be hard to verify the intralymphatic location of a labeled cancer cell. Furthermore, to thoroughly understand the relationship between intralymphatic cancer cell migration and lymphatic drainage rates, it is also necessary to map out draining lymphatic basins *in vivo* and follow cancer cell migration (5,24).

MRI with SPIO has the advantage of high sensitivity and whole body/organ imaging. However, since gradient echo sequences are very sensitive to local magnetic field disturbances induced by SPIO, dark signals from SPIO-labeled cells are generally larger than actual cancer cells or clusters (the so-called ‘blooming effect’) (25), leading to overestimation of the number of labeled cells distributing within target organs. Furthermore, this dark signal caused by shortened T_2* can also emanate from micro-hemorrhage or tiny air bubbles that also induce a similar susceptibility effect.

In this study, in addition to MR cell labeling and counterlabeling of the lymphatics, we employed optical imaging agents, QD. MRI demonstrated macro-distribution of target cancer cells in the whole body, while optical imaging was limited to a small field of view but gave insight into the micro-distribution of cancer cells within lymph nodes. Taken together, multimodal cell tracking method can compensate for the disadvantages of each modality. Several studies of dual-labeled cells were reported with stem cells using a combination of MRI and optical imaging (26,27). In these studies, stem cells were dual-labeled with MRI contrast agents and fluorophores, and then *in vivo* MRI demonstrated distribution and migration of labeled stem cells in injured spinal cord or carotid, followed by *ex vivo* fluorescence microscopy of sectioned tissue specimens, which showed the micro-distribution of the labeled cells within the target organ. In this study, we showed dual-labeled cancer cells tracking in the lymphatic system, which allowed minimally invasive MR imaging along with more intrusive but higher resolution intravital real-time optical imaging.

The viability of dual-labeled and SPIO-labeled cancer cells was slightly lower than that of nonlabeled control cells in this study. SPIO labeling with protamine sulfate and QD cell labeling have been reported not to influence cell viability at least in the short term (28–31). Therefore, it is unlikely that SPIO or QD were directly cytotoxic. It is more likely that the repeated intensive cell washing after SPIO labeling and multistep cell labeling process used here caused a small decrease in viability. More optimal SPIO labeling (29) or single-step dual-labeling (32) may improve the viability of dual-labeled cells, although additional newly synthesized duallabeling chemicals are required to achieve this alternative.

A lymphatic imaging agent, Gd-G6, was used to simultaneously image the lymphatics and the SPIO-labeled cells (2,33). Gd-G6 is a positive contrast agent on T_1w-FFE and b-FFE sequences, and as a result lymphatic basins were positively enhanced. The larger size of the G6 dendrimer scaffold results in gains in R_1 compared with small-molecule Gd chelates. Previously, cancer cells have been imaged with optical probes, including a combination of QD-labeled cancer cells and fluorophore-conjugated dendrimers (34), or fluorescence-protein-labeled cancer cells and fluorophore-conjugated monoclonal antibody (24). Our result demonstrated that MRI with a negative (SPIO) labeled cell and a positive (Gd-G6) labeled lymphatic system is capable of visualizing early micrometastastic deposits of cancer cells in lymph nodes. To evaluate lymphangiogenesis between lymphatic function and cancer cell migration, simultaneous visualization of both the cells and the lymphatics is important. It is note-worthy that the cancer cells entered the node through specific afferent lymphatics in the lymph node periphery, leaving the remainder of the node unaffected (34). The peripheral distribution of tumor cells at the early time point after injection is consistent with a previous report using fluorescence microscopy to visualize QD labeled cells. Subsequently, the tumor cells became more evenly distributed through the node (34). Preventing dissemination at this point may be useful in reducing the spread of cancer.

4. CONCLUSIONS

In conclusion, we demonstrate the ability to track early micrometastases of dual-labeled cells within the lymph nodes. With this method, both the lymphatics and labeled cancer cells within the lymphatics were simultaneously visualized, and intravital optical imaging confirmed the presence of cells using high-spatial-resolution *in vivo* microscopy in real time. These images can provide detailed information on migrating cancer cells within the lymphatic system as well as the relationship between regional lymphatic drainage function and cancer cell migration *in vivo*. This method is potentially a powerful research tool for investigating lymphatic metastases in animal models.

5. EXPERIMENTAL

5.1. Synthesis of gadolinium-dendrimer-based MRI contrast agent (Gd-G6)

A generation-6 polyamidoamine dendrimer (PAMAM-G6, 58 kDa; Sigma-Aldrich, St Louis, MO, USA) was coupled with the chelate 2-(p-isothiocyanatobenzyl)-6-methyl-diethylenetriamine-pentaacetic acid (1B4M) and 204 Gd(III) ions to obtain the Gd-G6 MRI contrast agent (220 kDa, ~10 nm in hydrodynamic diameter) for MR lymphangiography. The details of this Gd-G6 synthesis and quality control were described previously (2,35).

5.2. Cell line and cell culture

An established human breast cancer cell line, MDA-MB468 (36), was used for this study. The cell line was grown in RPMI 1640 medium (Invitrogen Corporation, Carlsbad, CA, USA) containing 10% fetal bovine serum (FBS; Invitrogen Corporation), 0.03% L-glutamine at 37 °C, 100 units ml^{-1} penicillin and 100 μg ml^{-1} streptomycin in 5% CO_2.

5.3. Labeling of cancer cells

Optical (QD) cancer-cell labeling was performed with Qtracker 655 (Invitrogen Corporation) following the manufacturer's protocol. The hydrodynamic diameter of QD655 is ~20 nm. Briefly, 10×10^6 MDA-MB468 cancer cells were suspended in 20 nM Qtracker 655 solutions, and then incubated for 2 h in 5% CO_2 at 37 °C. After incubation, QD-labeled-cancer cells were washed with complete medium three times and re-suspended with complete medium in a T-75 flask.

SPIO labeling was performed using the protamine sulfate method (31,37). Commercially available ferumoxide suspension (Feridex IV; Berlex Laboratories, Montville, NJ, USA) and protamine sulfate (American Pharmaceuticals Partners, Shaumburg, IL, USA) were used. Ferumoxide at a concentration of 100 μg ml^{-1} was placed in a tube containing serum-free RPMI 1640 medium (Invitrogen Corporation) and 0.03% L-glutamine. Protamine sulfate was then added to the solution at the concentration of 5 μg ml^{-1}. The solution containing ferumoxides and protamine sulfate was mixed for 5–10 min. After 5–10 min, an equal volume of the solution containing ferumoxide–protamine complexes was added to the existing complete media in the QD-labeled cell culture, followed by overnight incubation in 5% CO_2 at 37 °C. Then, labeled cancer cells were harvested by trypsinization and washed three times with PBS containing 10 U ml^{-1} heparin sulfate. Further, to eliminate unincorporated ferumoxide–protamine complexes thoroughly, collected cells were re-suspended in complete media for 8 h, and then only adherent cells on the flask bottom were harvested and washed with ice-cold PBS twice.

5.4. *In vitro* validation of dual-labeled cancer cells

5.4.1. Validation of dual labeling—To validate dual-labeling of cancer cells, fluorescence microscopy and Prussian blue staining were performed (38). Dual-labeled cells were smeared on a glass slide, and examined with fluorescence microscopy (BX61, Olympus America Inc., Melville, NY, USA) using RFP filter settings (excitation 560/55; emission 645/75 nm) to identify incorporated QD within the cell cytoplasm. Prussian blue staining of another slide was carried out to detect SPIO (Iron Stain Kit, Sigma-Adlrich). Additionally, flow cytometry was performed to assess the efficiency of dual labeling. One-million dual-labeled cells were treated with Cytofix/Cytoperm kit (BD, Franklin Lakes, NJ, USA) following the manufacturer's protocol, and then dextran immunostaining was performed using anti-dextran FITC-conjugated mouse monoclonal antibody (Stem Cell Technologies, Vancouver, Canada). Two-color flowcytometry was performed on a FACSCaliber (BD) and analyzed using CellQuest software (BD). These experiments were repeated three times.

5.4.2. Intracellular Iron Quantification—Quantification of intracellular iron labeled cells was performed using UV–vis spectrometric methods (39,40). After duallabeling, 5×10^5 dual-labeled cells were centrifuged at 3000 rpm for 5 min. After discarding the supernatants, cell pellets were incubated at 90 °C overnight (no cap on tubes). The next day, iron was dissolved by adding 1 ml of 5 M hydrochloric acid (HCl) to each tube and samples were further incubated at 60 °C for 4 h. During this incubation step, tubes were capped to prevent acid evaporation. After the incubation, 0.5 ml solution from each tube was

transferred to a separate 1.5 ml cuvette, and 0.5 ml freshly prepared 5% potassium ferrocyanide (Sigma-Aldrich) was added to each cuvette and incubated at room temperature in dark for 35 min. Prussian blue color developed in the reaction of the mixtures and became stable after 35 min. After 35 min, the absorbance was measured using a UV–vis spectrometer (8453 Value UV–vis Value System; Agilent Technologies, Santa Clara, CA, USA). The absorption profile of 200–1100 nm wavelengths was plotted to determine the peak absorbance wavelength. The peak absorbance for solution containing iron was 700 nm. Iron concentration in the sample was calculated from a standard curve that was derived from calibration standards of ferumoxides containing 0–10 μg ml^{-1} iron in the same acid mixture. Iron concentration was expressed as an average picograms of iron per cell. A total of five samples of dual-labeled cells or control cells were evaluated.

5.4.3. Trypan blue viability assay—Dual-labeled cells or control nonlabeled cells were suspended in PBS at the concentration of 10×10^6 ml^{-1} and mixed with 0.4% trypan blue dye at the 1:1 ratio. Ten microliters of this mixture was loaded into hemocytometer, after which cells were counted. Cells with an intact membrane excluded the dye and were considered as live cells. The percentage of live and dead cells was determined with 18 samples of dual-labeled or control cells each.

5.5. Intralymphatic cancer cell tracking with MR and optical imaging *in vivo*

All procedures were approved by the National Cancer Institute Animal Care and Use Committee. Female nude mice (National Cancer Institute Animal Production Facility, Frederick, MD, USA) were anesthetized via intraperitoneal injection of 1.15 mg sodium pentobarbital (Nembutal Sodium Solution, Ovation Pharmaceuticals Inc., Deerfield, IL, USA). Two million dual-labeled cancer cells were suspended in ice-cold PBS, and intracutaneously injected into the left paw of anesthetized mice 24 h prior to imaging.

In vivo MR imaging was performed using a 3 T clinical MRI scanner (Achieva, Phillips) with an inhouse 1-inch saddle type coil. Mouse was anesthetized with 3% isofluorane with oxygen and then placed on a mouse cradle and put into the MR coil in the prone position. Body temperature was kept around 36 °C using a heating pad. Then, MR images were acquired with respiratory triggering: a 3D T_1-weighted gradient echo sequence (T_1w-FFE) with fat suppression (slice thickness, 0.6 mm; number of excitations, 5; field of view, 8 × 8 cm; matrix, 512 × 512; repetition time, 16 ms; echo time, 2.302 ms; flip angle, 30°), and 3D-balanced-steady-state free precession (b-FFE) sequence (slice thickness, 0.6 mm; number of excitations, 8; field of view, 8 × 8 cm; matrix, 512 × 512; repetition time, 8.796 ms; echo time, 2.492 ms; flip angle, 45°). After MR image acquisition, 10 μl of 30 mM G6-Gd solution was intracutaneously injected at the left paw, where labeled cancer cells were inoculated, and another set of MR images were acquired 5–10 min after G6-Gd administration.

After MRI, the mouse underwent *in vivo* optical imaging. Mice were anesthetized via intraperitoneal injection of 1.15mg sodium pentobarbital (Nembutal Sodium Solution, Ovation Pharmaceuticals Inc., Deerfield, IL, USA), and the skin above left axillary lymph node was removed. Fluorescence images were obtained using a macro-zoom fluorescence

microscope (MVX10 Macroview, Olympus America, Center Valley, PA, USA) with GFR filter setting (excitation 470/40nm; emission, 525nm, long-pass) and recorded with a CCD video camera system (FluorVivo Mag, INDEC Biosystems, Santa Clara, CA, USA) in real-time.

After all imaging procedures, mice were euthanized with carbon dioxide, and the left axillary lymph node chain of each mouse was harvested and then subjected to histological validation with H-E staining, Prussian-blue staining and fluorescence microscopic images (BX61, Olympus). These experiments were repeated five times and showed consistent results in all mice. The *in vivo* imaging protocol is summarized in Fig. 2(A).

Supplementary Material

Refer to Web version on PubMed Central for supplementary material.

Acknowledgments

This research was supported by the Intramural Research Program of the National Institutes of Health, National Cancer Institute, Center for Cancer Research.

REFERENCES

1. Barrett T, Choyke PL, Kobayashi H. Imaging of the lymphatic system: new horizons. Contrast Media Mol Imag 2006; 1(6): 230–245.
2. Kobayashi H, Kawamoto S, Sakai Y, Choyke PL, Star RA, Brechbiel MW, Sato N, Tagaya Y, Morris JC, Waldmann TA. Lymphatic drainage imaging of breast cancer in mice by micro-magnetic resonance lymphangiography using a nano-size paramagnetic contrast agent. J Natl Cancer Inst 2004; 96(9): 703–708. [PubMed: 15126607]
3. Kim S, Lim YT, Soltesz EG, De Grand AM, Lee J, Nakayama A, Parker JA, Mihaljevic T, Laurence RG, Dor DM, Cohn LH, Bawendi MG, Frangioni JV. Near-infrared fluorescent type II quantum dots for sentinel lymph node mapping. Nat Biotechnol 2004; 22(1): 93–97. [PubMed: 14661026]
4. Ballou B, Ernst LA, Andreko S, Harper T, Fitzpatrick JA, Waggoner AS, Bruchez MP. Sentinel lymph node imaging using quantum dots in mouse tumor models. Bioconjug Chem 2007; 18(2): 389–396. [PubMed: 17263568]
5. Hoshida T, Isaka N, Hagendoorn J, di Tomaso E, Chen YL, Pytowski B, Fukumura D, Padera TP, Jain RK. Imaging steps of lymphatic metastasis reveals that vascular endothelial growth factor-C increases metastasis by increasing delivery of cancer cells to lymph nodes: therapeutic implications. Cancer Res 2006; 66(16): 8065–8075. [PubMed: 16912183]
6. Liu W, Frank JA. Detection and quantification of magnetically labeled cells by cellular MRI. Eur J Radiol 2009; 70(2): 258–264. [PubMed: 18995978]
7. Cheng WZ, Zeng MS, Yan FH, Rao SX, Shen JZ, Chen CZ, Zhang SJ, Shi WB. Ferucarbotran versus Gd-DTPA-enhanced MR imaging in the detection of focal hepatic lesions. Wld J Gastroenterol 2007; 13(36): 4891–4896.
8. Kobayashi H, Brechbiel MW. Nano-sized MRI contrast agents with dendrimer cores. Adv Drug Deliv Rev 2005; 57(15): 2271–2286. [PubMed: 16290152]
9. Bryant LH Jr., Brechbiel MW, Wu C, Bulte JW, Herynek V, Frank JA. Synthesis and relaxometry of high-generation (G = 5, 7, 9, and 10) PAMAM dendrimer–DOTA–gadolinium chelates. J Magn Reson Imag 1999; 9(2): 348–352.
10. Kosaka N, McCann TE, Mitsunaga M, Choyke PL, Kobayashi H. Realtime optical imaging using quantum dot and related nanocrystals. Nanomedicine (Lond) 2010; 5(5): 765–776. [PubMed: 20662647]

11. Kobayashi H, Longmire MR, Ogawa M, Choyke PL, Kawamoto S. Multiplexed imaging in cancer diagnosis: applications and future advances. Lancet Oncol 2010; 11(6): 589–595. [PubMed: 20338808]
12. Ogawa M, Regino CA, Seidel J, Green MV, Xi W, Williams M, Kosaka N, Choyke PL, Kobayashi H. Dual-modality molecular imaging using antibodies labeled with activatable fluorescence and a radionuclide for specific and quantitative targeted cancer detection. Bioconjug Chem 2009; 20(11): 2177–2184. [PubMed: 19919110]
13. Kosaka N, Ogawa M, Longmire MR, Choyke PL, Kobayashi H. Multi-targeted multi-color in vivo optical imaging in a model of disseminated peritoneal ovarian cancer. J Biomed Opt 2009; 14(1): 014023. [PubMed: 19256711]
14. Kosaka N, Ogawa M, Sato N, Choyke PL, Kobayashi H. In vivo realtime, multicolor, quantum dot lymphatic imaging. J Invest Dermatol 2009; 129(12): 2818–2822. [PubMed: 19536144]
15. Singletary SE, Connolly JL. Breast cancer staging: working with the sixth edition of the AJCC Cancer Staging Manual. CA Cancer J Clin 2006; 56(1): 37–47; quiz 50–31. [PubMed: 16449185]
16. Rizk N, Venkatraman E, Park B, Flores R, Bains MS, Rusch V. The prognostic importance of the number of involved lymph nodes in esophageal cancer: implications for revisions of the American Joint Committee on Cancer staging system. J Thorac Cardiovasc Surg 2006; 132(6): 1374–1381. [PubMed: 17140960]
17. Stacker SA, Achen MG, Jussila L, Baldwin ME, Alitalo K. Lymphan-giogenesis and cancer metastasis. Nat Rev Cancer 2002; 2(8):573–583. [PubMed: 12154350]
18. Arbab AS, Frank JA. Cellular MRI and its role in stem cell therapy. Regen Med 2008; 3(2): 199–215. [PubMed: 18307404]
19. Hoffman RM. Imaging cancer dynamics in vivo at the tumor and cellular level with fluorescent proteins. Clin Exp Metastasis 2009; 26(4): 345–355. [PubMed: 18787963]
20. Bulte JW, Duncan ID, Frank JA. In vivo magnetic resonance tracking of magnetically labeled cells after transplantation. J Cereb Blood Flow Metab 2002; 22(8): 899–907. [PubMed: 12172375]
21. Sadek H, Latif S, Collins R, Garry MG, Garry DJ. Use of ferumoxides for stem cell labeling. Regen Med 2008; 3(6): 807–816. [PubMed: 18947305]
22. Dahnke H, Schaeffter T. Limits of detection of SPIO at 3.0 T using T2 relaxometry. Magn Reson Med 2005; 53(5): 1202–1206. [PubMed: 15844156]
23. Shapiro EM, Sharer K, Skrtic S, Koretsky AP. In vivo detection of single cells by MRI. Magn Reson Med 2006; 55(2): 242–249. [PubMed: 16416426]
24. McElroy M, Hayashi K, Garmy-Susini B, Kaushal S, Varner JA, Moossa AR, Hoffman RM, Bouvet M. Fluorescent LYVE-1 antibody to image dynamically lymphatic trafficking of cancer cells in vivo. J Surg Res 2009; 151(1): 68–73. [PubMed: 18599080]
25. Bulte JW, Douglas T, Witwer B, Zhang SC, Strable E, Lewis BK, Zywicke H, Miller B, van Gelderen P, Moskowitz BM, Duncan ID, Frank JA. Magnetodendrimers allow endosomal magnetic labeling and in vivo tracking of stem cells. Nat Biotechnol 2001; 19(12): 1141–1147. [PubMed: 11731783]
26. Shen J, Zhong XM, Duan XH, Cheng LN, Hong GB, Bi XB, Liu Y. Magnetic resonance imaging of mesenchymal stem cells labeled with dual (MR and fluorescence) agents in rat spinal cord injury. Acad Radiol 2009; 16(9): 1142–1154. [PubMed: 19660710]
27. Cao AH, Shi HJ, Zhang Y, Teng GJ. In vivo tracking of dual-labeled mesenchymal stem cells homing into the injured common carotid artery. Anat Rec (Hoboken) 2009; 292(10): 1677–1683. [PubMed: 19685506]
28. Voura EB, Jaiswal JK, Mattoussi H, Simon SM. Tracking metastatic tumor cell extravasation with quantum dot nanocrystals and fluorescence emission-scanning microscopy. Nat Med 2004; 10(9): 993–998. [PubMed: 15334072]
29. Janic B, Rad AM, Jordan EK, Iskander AS, Ali MM, Varma NR, Frank JA, Arbab AS. Optimization and validation of FePro cell labeling method. PLoS One 2009; 4(6): e5873. [PubMed: 19517015]
30. Jaiswal JK, Mattoussi H, Mauro JM, Simon SM. Long-term multiple color imaging of live cells using quantum dot bioconjugates. Nat Biotechnol 2003; 21(1): 47–51. [PubMed: 12459736]

31. Arbab AS, Yocum GT, Kalish H, Jordan EK, Anderson SA, Khakoo AY, Read EJ, Frank JA. Efficient magnetic cell labeling with protamine sulfate complexed to ferumoxides for cellular MRI. Blood 2004; 104(4): 1217–1223. [PubMed: 15100158]
32. Vuu K, Xie J, McDonald MA, Bernardo M, Hunter F, Zhang Y, Li K, Bednarski M, Guccione S. Gadolinium-rhodamine nanoparticles for cell labeling and tracking via magnetic resonance and optical imaging. Bioconjug Chem 2005; 16(4): 995–999. [PubMed: 16029042]
33. Kobayashi H, Kawamoto S, Choyke PL, Sato N, Knopp MV, Star RA, Waldmann TA, Tagaya Y, Brechbiel MW. Comparison of dendrimer-based macromolecular contrast agents for dynamic micro-magnetic resonance lymphangiography. Magn Reson Med 2003; 50(4): 758–766. [PubMed: 14523962]
34. Kobayashi H, Ogawa M, Kosaka N, Choyke PL, Urano Y. Multicolor imaging of lymphatic function with two nanomaterials: quantum dot-labeled cancer cells and dendrimer-based optical agents. Nanomedicine (Lond) 2009; 4(4): 411–419. [PubMed: 19505244]
35. Kobayashi H, Sato N, Hiraga A, Saga T, Nakamoto Y, Ueda H, Konishi J, Togashi K, Brechbiel MW. 3D-micro-MR angiography of mice using macromolecular MR contrast agents with polyamidoamine dendrimer core with reference to their pharmacokinetic properties. Magn Reson Med 2001; 45(3): 454–460. [PubMed: 11241704]
36. Brinkley BR, Beall PT, Wible LJ, Mace ML, Turner DS, Cailleau RM. Variations in cell form and cytoskeleton in human breast carcinoma cells in vitro. Cancer Res 1980; 40(9): 3118–3129. [PubMed: 7000337]
37. Frank JA, Anderson SA, Kalsih H, Jordan EK, Lewis BK, Yocum GT, Arbab AS. Methods for magnetically labeling stem and other cells for detection by in vivo magnetic resonance imaging. Cytotherapy 2004; 6(6): 621–625. [PubMed: 15773025]
38. Koncki R Chemical sensors and biosensors based on Prussian blues. Crit Rev Anal Chem 2002; 32(1): 79–96.
39. Rad AM, Janic B, Iskander AS, Soltanian-Zadeh H, Arbab AS. Measurement of quantity of iron in magnetically labeled cells: comparison among different UV/VIS spectrometric methods. Biotechniques 2007; 43(5): 627–628, 630, 632 passim. [PubMed: 18072592]
40. Boutry S, Forge D, Burtea C, Mahieu I, Murariu O, Laurent S, Vander Elst L, Muller RN. How to quantify iron in an aqueous or biological matrix: a technical note. Contrast Media Mol Imag 2009; 4(6): 299–304.

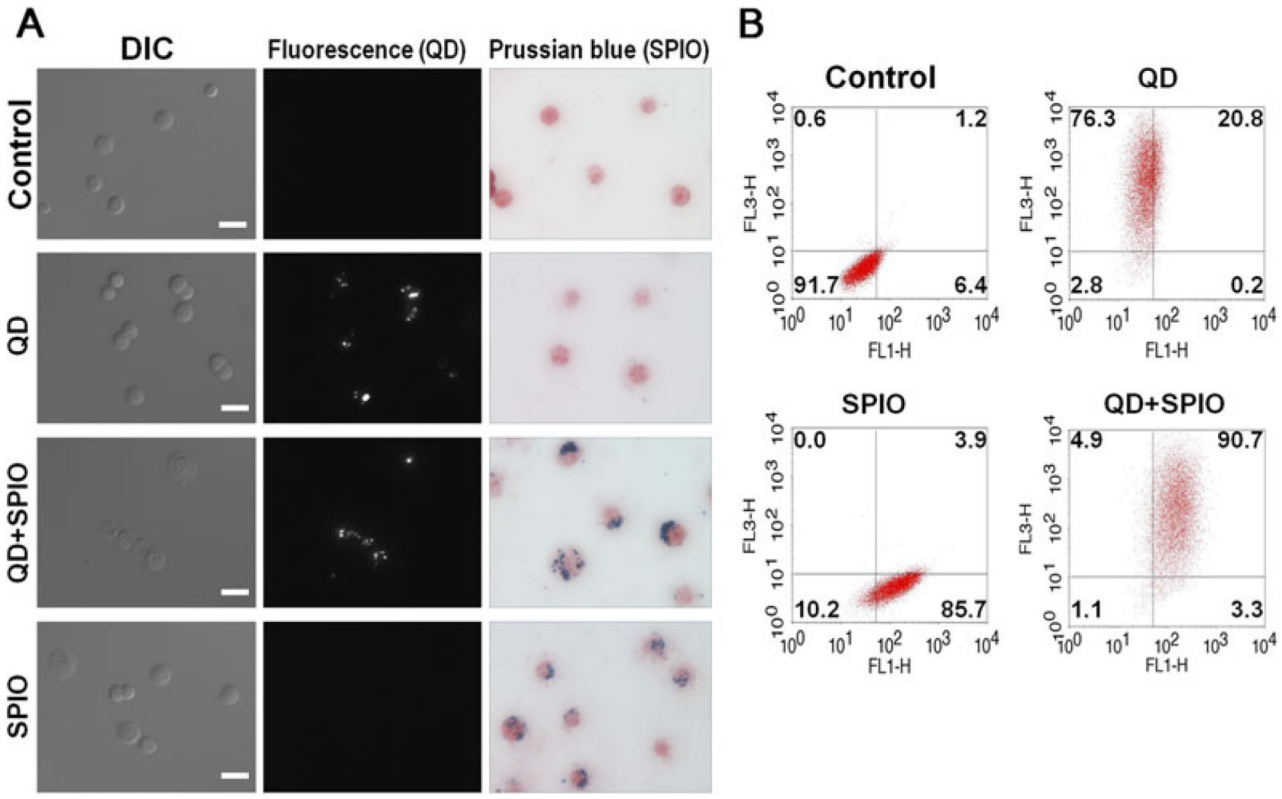

Figure 1.

In vitro validation of dual-labeling of MDA-MB468. (A) Differential interference contrast (DIC) images, fluorescence images and Prussian blue staining of dual-labeled MDA-MB468. Scales in DIC are 25 μm. (B) Flow cytometory with dextran staining (SPIO staining) of dual-labeled MDA-MB468. Argon ion laser (488 nm) was used for excitation with FL1 emission filter (530/30 nm) for anti-dextran FITC-conjugated antibody and FL3 (650 nm long-pass) for quantum dot 655.

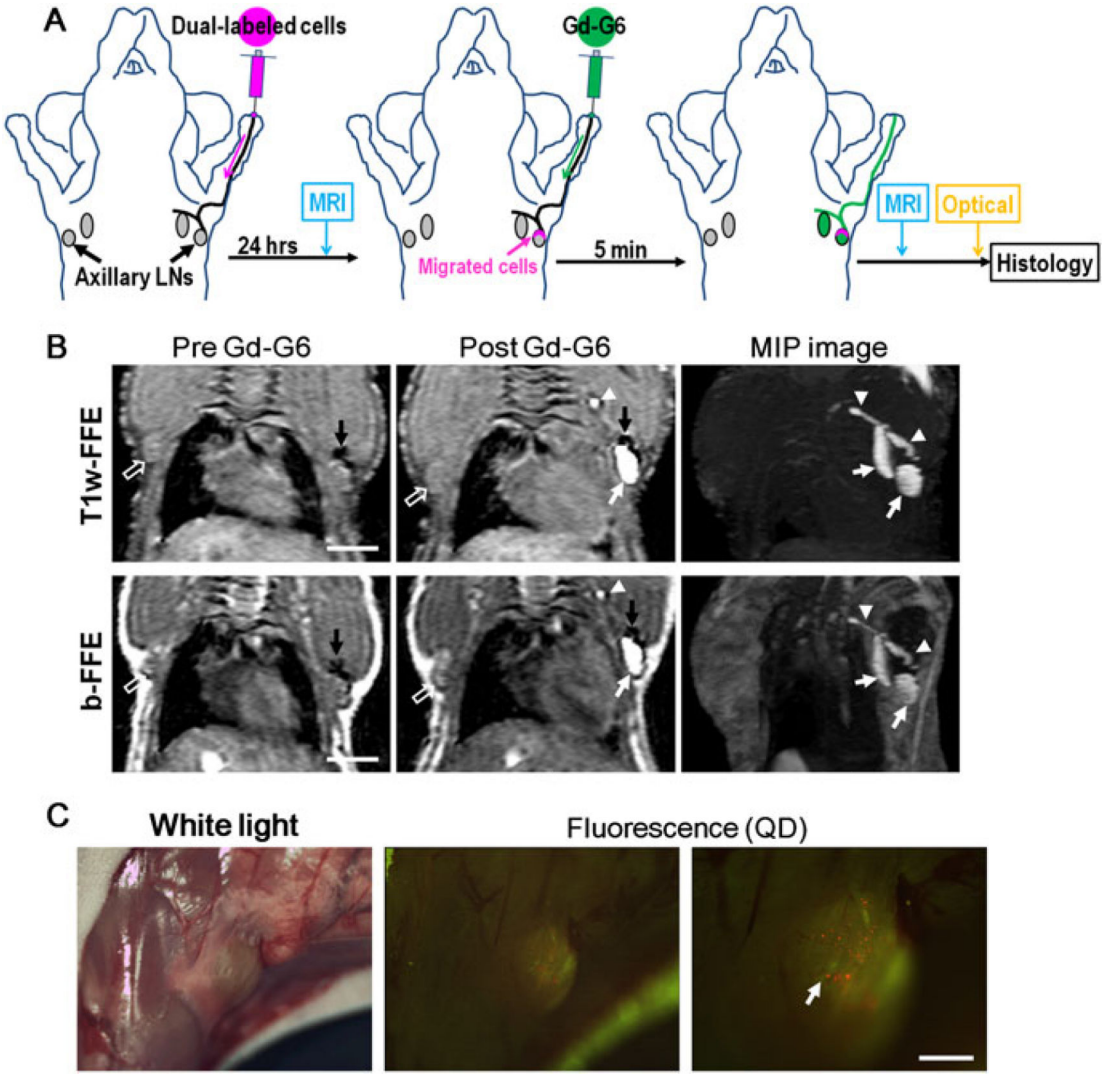

Figure 2.

Intralymphatic cancer cell tracking with MR and optical imaging *in vivo.* (A) Schematic illustration of the protocol. (B) Both T_1-weighted-gradient echo sequence (T_1w-FFE) and balanced-steady-state free precession (b-FFE) images show iron-labeled cancer cells in the periphery of the left axillary lymph node (dark areas, black arrows). After administration of Gd-G6 MR contrast agents into the left paw, the cancer cells and lymphatic basin are simultaneously depicted (lymph nodes: white arrows, lymphatic ducts: arrow heads), while no enhancements (neither negative nor positive) are observed in the contralateral axillary lymph node (open arrows). MIP, maximum intensity projection. Scales in images are 5 mm. (C) *In vivo* fluorescence images show optically labeled cancer cells (small red dots, arrow) in an axillary lymph node with high spatial resolution. Note that the green fluorescence arises from autofluorescence in the background tissue. Scale in fluorescence image is 1 mm. These cancer cells can be observed in real time (see video in Supporting Information).

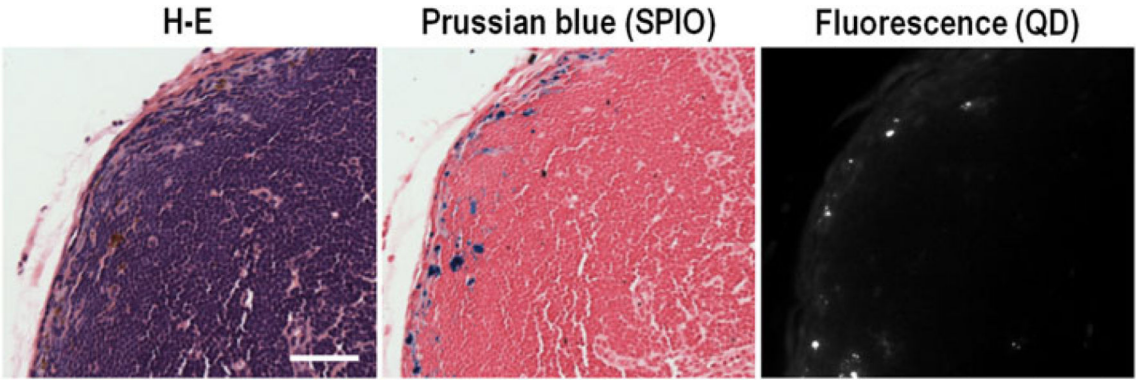

Figure 3.

Histological validation of the removed left axillary lymph node. Labeled cancer cells are found in the peripheral of lymph node in Prussian-blue staining (blue dots) and fluorescence images (white dots). Scale in H-E staining is 50 μm.